Mechanics and Mechanical Engineering
Vol. 20, No. 4 (2016) 531–552

On a Hybrid Approach for Modeling and FEM Analysis of Body Collision in an Engineering Application

Mariusz Warzecha
Department of Mechanics and Vibroacustics
AGH University of Science and Technology
mwarzech@agh.edu.pl

Received (29 September 2016)
Revised (6 October 2016)
Accepted (11 Novenber 2016)

A methodology for hybrid modeling and FEM analysis of body collision is presented and illustrated by a simplified, theoretical example. Each step required to use the presented approach in engineering practice is described and methods of checking the correctness of conducted FEM analysis are given. The influence of colliding body configuration on the value of maximal collision force is studied and discussed. The results of FEM analysis, using the suggested approach, supported by free software, are presented and their correctness is verified by proposed checking methods. Advantages and disadvantages of the proposed approach are also discussed.

Keywords: collision models, Code–Aster, FEM analysis, impact simulation.

1. Introduction

An eccentric collision between colliding bodies occurs when mass centers of one of the colliding body or both of them do not lie on the impact line. It is a straight line which passes through a contact point and is normal to plane tangential to surfaces of colliding bodies in the contact point, so it is, in case of absence of friction, collinear with $\mathbf{F}_1$ and $\mathbf{F}_2$ vectors shown in Fig 1. Eccentric collisions can be found in nature, i.e. in astrophysics - asteroids hitting planets or rubble pile asteroids collisions, as well as in technical and industrial processes, i.e. a collision between an axle set of a rail–vehicle and a unevenness of a track [1], an aircraft landing, a shakeout of solidified castings when removing from sand molds etc. It is often recognized in industries like defense, mining or building.

A collision is complex dynamic phenomenon, the modeling and simulation of which requires taking many properties of colliding bodies, such as material, geometry and velocity, into consideration. Approaches for the modeling collision at the actual state of the art can be divided into impulse-momentum and time dependent.

In the first approach the collision time is neglected and the concept of the restitution coefficient, for calculating kinematic quantities of colliding bodies, is used. There are various methods of defining the coefficient of restitution: Newton's defining relationship between the normal components of the velocities before and after the collision at the contact point [2], Poisson's defining relationship between force impulse in compression and restitution phases of the collision [3] and Stronge's use of square root of the ratio of energy released during restitution phase to the energy absorbed during the compression phase of collision [4]. Because the coefficient of restitution shows the dependence on the body shape in the region of collision, their mass and velocity it is convenient to use the concept of energy flux density proposed for the central collision by Bagrejev [5]. The energy flux density Φ combines factors that influence the value of restitution coefficient mentioned in previous sentence (refer Eq. (14)) An empirically determined relation between the value of restitution coefficient and energy flux density Φ is useful for determining the value of restitution coefficient in a particular collision case. The time dependent models are describing an explicit relation between local deformation and forces acting on the colliding bodies. The loss of kinetic energy during the collision in time dependent models can be modeled by damping.

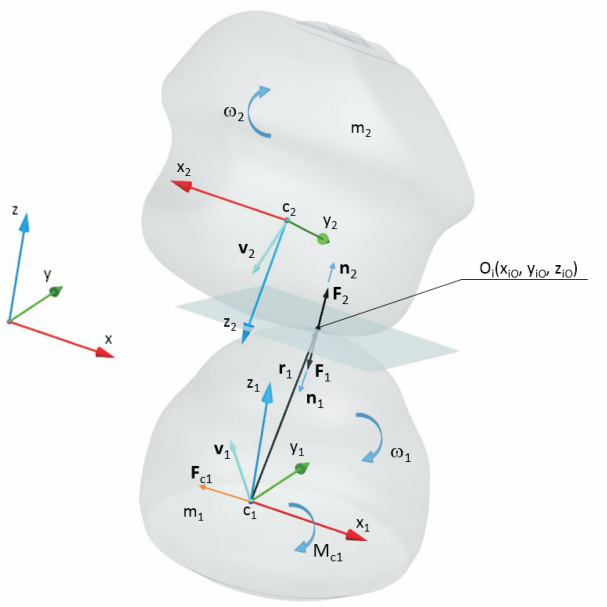

Figure 1 Eccentric collision of two bodies

This paper proposes a hybrid approach for modeling and simulating an eccentric collision of bodies. The meaning of "hybrid" can be understood on two levels: the first - it combines impulse-momentum and time dependent modelling of collision

in analytical calculations and the second - it combines analytical calculations with FEM analysis.

Hertz's contact model is used for determining force impulse in the collision compression phase. The concept of energy flux density [5] generalized in [6] is used for determining the restitution coefficient and the calculating impulse of force in the collision restitution phase. The maximal collision force dependence on the colliding body configuration is studied in the case of sphere colliding with ellipsoid. Calculated force functions are used in FEM analysis to present approach of removing one of colliding bodies from analysis and replacing it with directly applied, time dependent force. The analytical validation of the FEM results is presented. The results of an example analysis as well as advantages and potential disadvantages of proposed hybrid methodology are discussed.

2. Methodology

2.1. *Calculating force impulse in the compression phase for the central collision*

Hertz's-Stayerman's nonlinear spring model Eq. (1) is used as a starting point for the calculation of force impulse in the collision compression phase.

$$P = k_H x^n \tag{1}$$

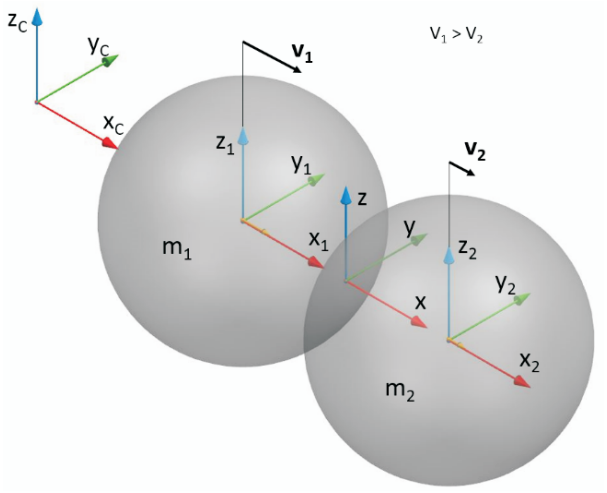

Figure 2 Central collision of two spheres

Constants k_H and n in Eq. (1) are depending on material and geometric properties of colliding bodies and can be calculated on the basis of elastostatic theory. Hertz–Stayerman model assumes that deformation occurs only in an area near the contact point and neglects elastic wave motion. Therefore, a description of interaction between colliding bodies via non–linear spring which is acting along the line of

impact, is possible. Using this model, a description of the motion of the two spheres presented in Fig. 2 leads to Eq. (2).

$$m_w\ddot{x} + k_H x^n = 0 \tag{2}$$

where: m_1, m_2 – masses of colliding spheres:

$$m_w = \frac{m_1 m_2}{m_1 + m_2} \tag{3}$$

$$x = x_1 - x_2 - (r_1 + r_2) \tag{4}$$

$$\dot{x} = \dot{x}_1 - \dot{x}_2 \tag{5}$$

$$\ddot{x} = \ddot{x}_1 - \ddot{x}_2 \tag{6}$$

Because of the nonlinearity of Eq. (2) there is no possibility for an easy and straightforward analytical solution, which will describe the changes of x in time. Therefore, in order to be able to describe it, the steps represented by Eq. (7) to (9) are taken.

$$\frac{d}{dt}(\dot{x}^2) = 2\dot{x}\ddot{x} = -2\dot{x}\frac{k_H x^n}{m_w} \tag{7}$$

Multiplying by dt and integrating leads to Eq. (8) :

$$\dot{x} = \sqrt{v_0^2 - \frac{2k_H x^n}{m_w} x^{n+1}} \tag{8}$$

After separating the variables, integrating again and taking into consideration the initial conditions $x(0) = 0$ Eq. (9) can be received:

$$\int \frac{1}{\sqrt{v_0^2 - \frac{2k_H x^n}{m_w} x^{n+1}}} dx = t \tag{9}$$

Introducing new variable:

$$z + \frac{x}{x_{max}}$$

and using special functions to describe the integral on the left side of Eq. (9), Eq. (10) can be written as:

$$t = \frac{v_0}{x_{max}} z \, {}_2F_1\left(\frac{1}{2},\ \frac{1}{n+1},\ 1 + \frac{1}{n+1},\ z^{n+1}\right) \tag{10}$$

where:

$$z \in < 0,\, 1 > \tag{11}$$

and

$${}_2F_1\left(\frac{1}{2},\ \frac{1}{n+1},\ 1 + \frac{1}{n+1},\ z^{n+1}\right) \tag{12}$$

represents the hypergeometric series.

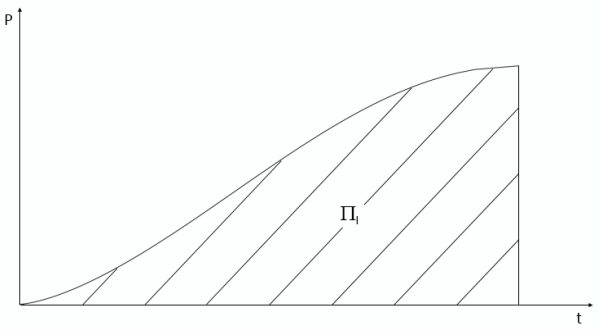

Figure 3 Relation of collision force against time

Using numerical methods, an inverse relation to Eq. (10) can be found and thus the relation of displacement during the collision against time can be determined. It is always possible as the function described by Eq. (10) is monotonic in its domain. Substituting this relation to Eq. (1) gives the relation of collision force against time. Determining the area beneath this relation as shown in Fig. 3 allows for determining force impulse Π_1 during the collision compression phase. Because of the energy transformations during the collision, an impulse Π_2, restored during the restitution process, will be smaller than the impulse Π_1. According to Poisson hypothesis, the correlation between the impulse Π_1 and the impulse Π_2 can be described using the coefficient of restitution, as shown in Eq. (13).

$$\Pi_2 = R\Pi_1 \tag{13}$$

In general, the coefficient of restitution is not a constant value but shows a dependence on the velocity, mass and shape of the colliding bodies in the vicinity of the contact area. To determine the value of the coefficient of restitution in a specific collision, it is convenient to use the energy flux density Φ during the collision, proposed for central collinear collision in [5].

$$\Phi = \frac{m_w v_w^2}{2r_w^3} \tag{14}$$

where:

m_w – reduced mass of colliding bodies, Eq. (3)

v_w – relative velocity of colliding bodies prior to collision ($\dot{x}_1 - \dot{x}_2$ for $t = 0$)

r_w – reduced radius of curvature in the contact point determined from Eq. (15)

$$r_w = \frac{r_i r_j}{r_i + r_j} \tag{15}$$

Using an empirical relation between the coefficient of restitution R against the density of energy flux Φ and calculating an impulse during compression phase Π_1 it is possible to calculate impulse during restitution phase Π_2. The knowledge about total impulse during the collision $\Pi = \Pi_1 + \Pi_2 = \Pi_1 + R\Pi_1$, where R is the coefficient of restitution, enables calculation of the kinematic parameters of the bodies after the collision.

2.2. *Generalization about eccentric collision*

To apply the approach presented in paragraph 2.1 for eccentric collision, the methodology proposed in [6] is used. It allows for the calculation of reduced mass at the collision point using Eq. (21). The starting point for calculating the reduced mass is the Euler Eq. (16). Refer to Fig. 1 for a better symbol understanding.

$$\mathbf{I_i}\frac{\mathrm{d}\omega_\mathbf{i}}{\mathrm{dt}} + \omega_\mathbf{i} \times \mathbf{I_i}\omega_\mathbf{i} = \mathbf{M_{ci}} + \mathbf{r_i} \times \mathbf{F} \tag{16}$$

where:

$i = 1, 2$ – index describing colliding bodies

$\mathbf{I_i}$ – tensor of inertia in the central reference frame $C_i x_i y_i z_i$ of i–th body

$\mathbf{M_{ci}}$ – external moment applied to body m_i

$$\mathbf{I_i} = \begin{bmatrix} I_{x_i} & -I_{x_i y_i} & I_{x_i z_i} \\ -I_{y_i x_i} & I_{y_i} & -I_{y_i z_i} \\ I_{z_i x_i} & I_{z_i y_i} & I_{z_i} \end{bmatrix} \tag{17}$$

Eq. (16) allows for determination of the derivative of angular velocity, which can be then substituted into Eq. (18) describing the acceleration of point O_i.

$$\mathbf{a_{O_i}} = \frac{\mathbf{F_i} + \mathbf{F_{ci}}}{\mathrm{m_i}} + \frac{\mathrm{d}\omega_\mathbf{i}}{\mathrm{dt}} \times \mathbf{r_i} + \omega \times (\omega_\mathbf{i} \times \mathbf{r_i}) \tag{18}$$

After substituting the derivative of angular velocity calculated from Eq.(16) into Eq. (18), neglecting limited value terms and getting the projection of acceleration $\mathbf{a_{Oi}}$ against the direction of the collision line, Eq. (19) can be written as:

$$\begin{aligned} a_{ni} = \mathbf{a_{O_i}}\mathbf{n_i} &= \left\{ \frac{\mathbf{F_i}}{\mathrm{m_i}} + [\mathbf{I_i^{-1}}(\mathbf{r_i} \times \mathbf{F_i})] \times \mathbf{r_i} \right\} \mathbf{n_i} \\ &= F_i \left\{ \frac{\mathbf{n_i}}{m_i} + [\mathbf{I_i^{-1}}(\mathbf{r_i} \times \mathbf{n_i})] \times \mathbf{r_i} \right\} \mathbf{n_i} \end{aligned} \tag{19}$$

Hence, the term presented by Eq. (20) can be considered:

$$m_{wi} = \frac{F_i}{a_{ni}} = \frac{1}{\left\{ \frac{\mathbf{n_i}}{m_i} + [I_i^{-1}(\mathbf{r_i} \times \mathbf{n_i})] \times \mathbf{r_i} \right\} \mathbf{n_i}} \qquad i = 1, 2 \tag{20}$$

After substituting Eq. (20) into Eq. (3) for both colliding bodies and assuming that x_i, y_i, z_i are the central principal axes of inertia of both colliding bodies,

Eq. (21) can be written.

$$
\begin{aligned}
m_w &= \frac{m_{w1}m_{w2}}{m_{w1}+m_{w2}} = \left[\frac{1}{m_{w1}}+\frac{1}{m_{w2}}\right]^{-1} \\
&= \left[\frac{1}{m_1}+\frac{1}{m_2}+\frac{1}{I_{x1}}(z_{1O}\mathbf{n_1j_1}-\mathrm{y_{1O}}\mathbf{n_1k_1})^2\right. \\
&+\frac{1}{I_{y1}}(z_{1O}\mathbf{n_1i_1}-\mathrm{x_{1O}}\mathbf{n_1k_1})^2+\frac{1}{\mathrm{I_{z1}}}(\mathrm{y_{1O}}\mathbf{n_1i_1}-\mathrm{x_{1O}}\mathbf{n_1j_1})^2 \\
&+\frac{1}{I_{x2}}(z_{2O}\mathbf{n_2j_2}-\mathrm{y_{2O}}\mathbf{n_2k_2})^2+\frac{1}{\mathrm{I_{y2}}}(\mathrm{z_{2O}}\mathbf{n_2i_2}-\mathrm{x_{2O}}\mathbf{n_2k_2})^2 \\
&\left.+\frac{1}{I_{z2}}(y_{2O}\mathbf{n_2i_2}-\mathrm{x_{2O}}\mathbf{n_2j_2})^2\right]^{-1}
\end{aligned}
\tag{21}
$$

where:

$\mathbf{n_i}$ – versors of line of impact, $i = 1, 2$

$\mathbf{i_i}$, $\mathbf{j_i}$, $\mathbf{k_i}$ – versors of central principal axes of inertia, $i = 1, 2$

x_{iO}, y_{iO}, z_{iO} – coordinates of point O, $i = 1, 2$

I_{xi}, I_{yi}, I_{zi} – central principal moments of inertia, $i = 1, 2$.

Therefore, Eq. (21) can replace Eq. (3) in paragraph 2.1 allowing for the calculation of the collision impulse in the eccentric collision. The reduced mass of the colliding bodies, calculated form Eq. (21), can also be used in Eq. (14) for calculation of the energy flux during the collision, which is needed to determine the coefficient of restitution.

Consider two bodies colliding as shown in Fig. 1. Both of them have no displacement constraints except for the fact that they are impenetrable at point O, where the contact occurs. The bodies have mass centers located at O_i , masses m_i and inertia tensors $\mathbf{I}_i$, $i = 1, 2$. Vector $\mathbf{r}_i$ locates point O respectively from O_i. Let $\mathbf{v}_i$ be the linear velocity of the mass center and ω_i the corresponding angular velocity. Knowing the impulse Π_i**,** changes of linear and angular velocity can be presented as follows:

$$\Delta v_1 = \frac{\Pi_i}{m_i} \tag{22}$$

$$\Delta\omega_i = I_i^{-1}\, r_i x \Pi_i) \tag{23}$$

2.3. *Numerical simulation*

Maximal force during the eccentric collision depends on the configuration of the colliding bodies to each other. For the investigation of the influence of colliding bodies configuration on maximal force during collision, a numerical simulation, using Python and freely available libraries, is implemented. To allow parametrization of a study, it has been decided to choose a shape, which can be described by an analytical equation. For its generality, an ellipsoid, described by Eq. (24) has been used:

$$\frac{x^2}{a^2} + \frac{y^2}{b^2} + \frac{z^2}{c^2} = 1 \tag{24}$$

where:
x, y, z – coordinates of Cartesian coordinate system
a, b, c – semi–principal axes of an ellipsoid

For given values of semi principal axes, the simulation automatically generates a cloud of points on its surface and stores them in matrix. At each of these points, the value of maximal force during collision with a sphere is determined. The sphere is always hitting along the line normal to an ellipsoid at the contact point. The versor of this line is determined from Eq. (25).

$$n = \frac{1}{\sqrt{\frac{4x_0^2}{a^4} + \frac{4y_0^2}{b^4} + \frac{4z_0^2}{c^4}}} \left[\frac{2x_0}{a^2}, \frac{2y_0}{b^2}, \frac{2z_0}{c^2} \right] \tag{25}$$

where:
x_0, y_0, z_0 – collision point coordinates
The friction during the collision is neglected. The parameters of the ellipsoid and sphere, needed for the calculation, can be easily defined as variables. Therefore, an effort needed to define material properties, velocities, masses etc. for both the ellipsoid and sphere is limited. The created simulation has the ability to graphically represent the results on a wireframe created in 3D space. The maximal collision force is represented by a circle having its central point at the collision point. The radius of this circle is proportional to the value of the maximal collision force at this point. Additionally, its color is darker with a decreasing value of the maximal collision force. An example of such a graphical representation is shown in Fig. 4. The results presented in this Figure are discussed in the concluding paragraph.

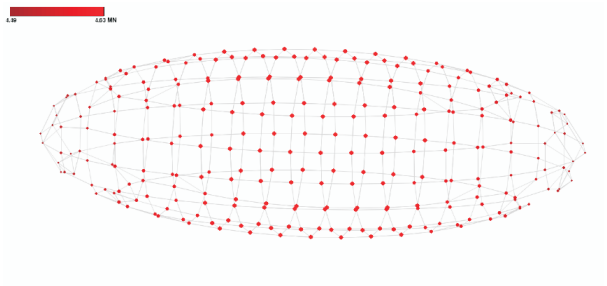

Figure 4 Example of a graphical representation implemented in a numerical simulation

For a determination of the Hertz constant (k_H in Eq. (1)) it is assumed, that the ellipsoid surface near the contact point can be approximated by a sphere. The radius of such a sphere is calculated as an average of the radiuses at the contact point of ellipses, created by cutting the ellipsoid with planes normal to the axes of

the main coordinate system and passing through the collision point. The radius of such an ellipse at the contact point can be evaluated from Eq. (26).

$$\frac{1}{R} = \frac{\alpha\beta}{(\alpha^2 \sin^2\gamma + \beta^2 \cos^2\gamma)^{\frac{3}{2}}} \tag{26}$$

where:
R – radius of the ellipse at a given point
α, ß – semi- principal axes of the ellipse created by cutting the ellipsoid with a plane perpendicular to one of main coordinate system axes,
γ – independent parameter having values from 0 to 2π

Simulation then uses Eq. (27) to separately determine the Hertz constant at each collision point:

$$k_H = \frac{4}{3} E_{red} \sqrt{R_{red}} \tag{27}$$

where:
E_{red} – reduced Young modulus, calculated from Eq. (28)
R_{red} – reduced Radius, calculated from Eq. (15)

$$\frac{1}{E_{red}} = \frac{1}{E_{ellipsoid}} + \frac{1}{E_{sphere}} \tag{28}$$

where:
$E_{ellipsoid}$– Young modulus of the material from which the ellipsoid is made
E_{sphere} – Young modulus of the material from which the sphere is made

$$\frac{1}{R_{red}} = \frac{1}{R} + \frac{1}{r} \tag{29}$$

where:
R – radius of the sphere approximating the ellipsoid at the collision point
r – radius of the colliding sphere.

A relation of the force against time acting during the collision at specified points can be evaluated by the simulation. Eq. (10) is used directly at the compression phase. For the restitution phase, the curve is iteratively approximated. As a base for this approximation Eq. (10) is taken, giving it physical justification. The parameters of this equation are evaluated iteratively. For each iteration an area beneath the force curve in the restitution phase is calculated and then compared with the force impulse obtained from Eq. (13). Iterations are stopped, when the difference is lower than 1%. Additionally, there is a constraint put on the approximated curve to be continuous with the curve calculated for the compression phase at a point, where the force reaches its maximal value. An example of the force relation in the time calculated by simulation is presented in Fig 5.

Coefficient of restitution required in Eq. (13) is calculated separately for each point using empirical Eq. (30) presented in [7].

$$R = 0,55 - 0,047 \ln\phi \qquad \text{for} \quad -5 < \ln\phi < 6 \tag{30}$$

where:
φ - density of energy flux calculated from Eq. (14).

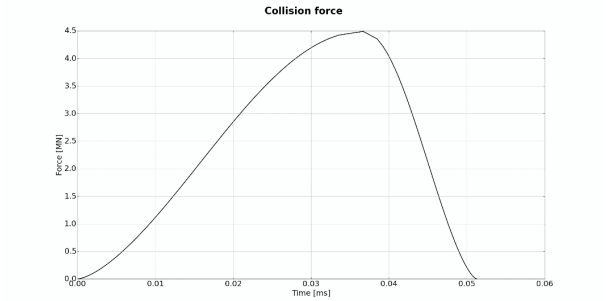

Figure 5 Example of relation of force acting during collision in time generated by simulation

At this point it has to be mentioned, that using Eq. (30) is limiting the material, from which the ellipsoid and sphere can be made of, to steel with a hardness of 1400 HB. To properly simulate the behavior of bodies made from other materials, a different relation has to be used.

The simulation has implemented two tests for checking the correctness of the conducted calculations. If one of them is not fulfilled, simulation returns error.

The first test uses the analytically calculated Eq. (31) to get the impulse of collision force during compression, assuming that the ellipsoid has no angular velocity. This analytical value is then compared with the numerically obtained value of the collision force impulse during the compression phase, which is obtained by a numerical integration of the relation similar to this presented in Fig. 5. The test is passed when the difference between both values is lower than 3 % . This error threshold is dictated by an error made by the numerical computation and its purpose is to avoid withdrawing of the correctly calculated values.

$$\Pi_1 = m_w v_w \tag{31}$$

where:
Π_1 – impulse of collision force during the compression phase
m_w– reduced mass of the ellipsoid and sphere at the collision point, calculated from Eq. (21)
v_w – relative velocity of the colliding bodies at the collision points prior to collision ($v_0^{sphere} - v_0^{ellipsoid}$ for $t = 0$)

The second test calculates the loss of kinetic energy during collision using the Carnot theorem and directly using the velocities of the bodies before and after the collision and subtracting the kinetic energy after collision from the kinetic energy before collision. If properly calculated both values should be the same. The loss of energy during collision according to the Carnot theorem is determined from Eq. (32).

$$\Delta E = \frac{1 - R^2}{2} m_w v_w^2 \tag{32}$$

To determine kinetic energy loss using velocities of bodies before and after collision, Eq. (22) and (23) are used to obtain changes in linear and angular velocity.

Simulation compares the value of energy loss obtained from the Carnot theorem with energy loss calculated directly from the differences and returns error if the difference is bigger than 1 %. If one of the above tests return error, the simulation is stopped and the user is required to investigate the reason and causes of the error.

2.4. *FEM transient analysis*

The solution of dynamic impact problems using finite element software makes an analyst face several challenges. Contact modeling, for which major part of algorithms, tests and literature is available, concerns quasi-static problems, not suitable for dynamic analysis, for which an additional time step is required. The necessity to introduce the contact between colliding bodies adds difficult non linearity into model. Several issues concerning taking into account the complex collision phenomena, generating proper mesh at area of contact or assessing the performance and capability of the available algorithms [8] can create difficulties, despite a literature review delivered in [9]

This article proposes an approach, which can eliminate some of the problems mentioned above. The idea is to remove the simulation of the collision contact from the FEM analysis and replace it with a directly applied collision force relation calculated by the numerical simulation as described in the paragraph 2.3. Such an approach has several advantages. It removes nonlinearity related to contact, allows for easier mesh generation, avoids problems with penetration and shortens the simulation time as the load is known prior to the simulation.

To present the proposed approach, the transient FEM analysis is conducted. The behavior of an ellipsoid shaped body hit by a sphere is investigated. This paragraph describes the applied methods, tools and the definition of analysis.

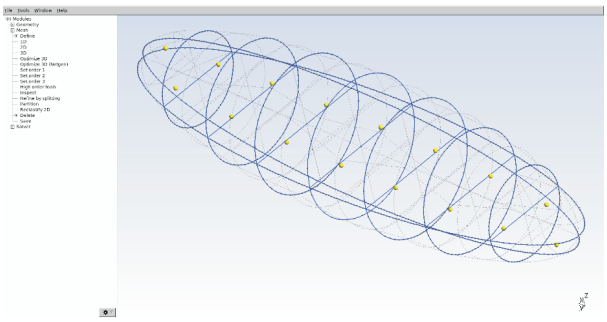

Figure 6 Geometry read by Gmsh from ASCII file

For 3D mesh generation and displaying the results Gmsh is used. [10] It is a lightweight, free software meshing tool allowing for parametric input and advanced visualization. Gmsh allows for an interaction using a graphical user interface or ASCII text files, containing instructions in Gmsh's own scripting language. For 3D mesh generation, for transient analysis the second option is used. The numerical

simulation described in paragraph 2.3 allows for the export of the geometry to an ASCII text file, which can then be read by Gmsh. An example of such imported geometry is presented in Fig. 6. The size of the generated mesh is prescribed in the input file for each point. The groups of nodes needed for applying the loads and plotting the graphs are defined manually using a graphical user interface. The generated mesh, the example of which is presented in Fig. 7, is exported to a file using MED mesh format, which is then used as an input to the FEM solver.

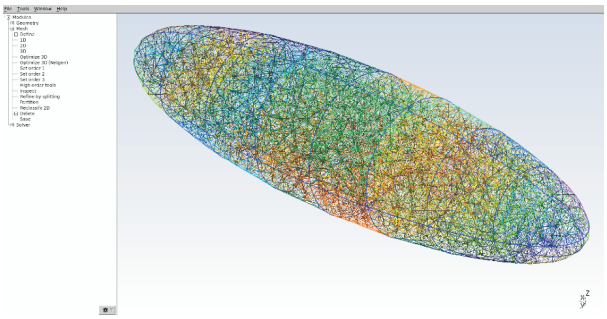

Figure 7 Mesh generated by Gmsh

To obtain the solution of a given problem, Code_Aster, a free software FEM numerical analysis program, is used. It has been developed by the French company EDF and after years of development has been published under a GNU GPL license. Code_Aster requires two inputs: the first is mesh, providing geometry of the body to be analyzed and the control file, providing information about the type of analysis, boundary conditions etc. The first input, mesh, is generated by Gmsh. The control file is created using text editor (EMACS). It contains instructions specific for Code_Aster. [11] A link between the control file and mesh is established by named groups of nodes and elements created in the MED file. The force acting during the collision is exported from the python numerical simulation described in paragraph 2.3. The curve, presented as an example in Fig. 5, is represented in the control file as a list of paired value. Each pair of values gives the value of time and the value of the collision force at that time. The force is always applied at a direction normal to the ellipsoid surface at a given point. There are no constraints on the ellipsoid displacement. A default setting of Code_Aster specifies calculation of displacements, velocities and accelerations at the mesh nodes. The control file additionally specifies von Mieses (Huber) reduced stresses as a required output to observe the stress levels caused by the collision. The results are written into a MED file, which can be then loaded into the Gmsh post processing module. Additionally, graphs are generated for specified nodes and the numerical values are exported into a text table, which can be read for example by any typical spreadsheet application. The results obtained from the simulation and read from the MED file into the Gmsh post processing module are presented in Fig. 8.

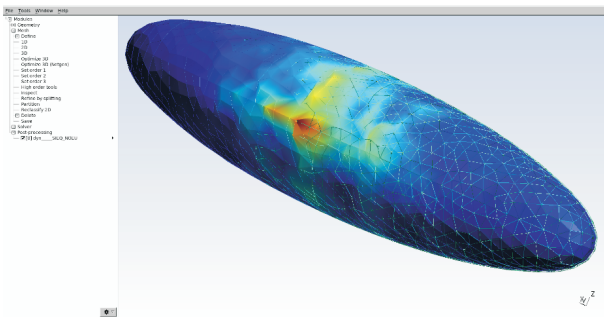

Figure 8 Results imported to Gmsh post processing module

Code_Aster is a command line program but it has a graphical manager, ASTK, which allows for running an analysis and the managing of multiple input and output files by interaction with a graphical user interface. ASTK is used for managing the analysis conducted in the scope of this article. To verify the correctness of the FEM analysis results, the values of the velocities obtained from it are compared with the values of the velocities, which can be calculated using impulses values obtained from the numerical simulation as described in the paragraph 2.3.

3. Results

3.1. *Influence of body configuration during collision on maximal collision force*

The implemented simulation, as described in paragraph 2.3, is used to investigate how the configuration of colliding bodies influences the maximal collision force. To eliminate the influence of the relative velocity at the collision point, the angular and linear velocity of an ellipsoid body is set to 0. This ensures that the relative velocity will not depend on the location where the ellipsoid body is hit, and will be equal to the linear velocity of the sphere, which always hits the ellipsoid body along normal to its surface at the collision point, as shown in Fig 9. A numerical experiment is structured as shown in Table 1. The impact of geometrical dimensions and colliding body masses is studied. For the purpose of this experiment, two semi-principal axes of ellipsoid are set to be equal (b and c) and axis a is changing to describe more narrow shapes, which vary more and more from a spherical shape, for which the given ratio equals 1. Additionally, for each geometrical ratio a different relation of colliding body masses is introduced. It is described by the ratio of the ellipsoid body mass m_1 to the hitting sphere body mass m_2. For example, the in cell for which the geometrical and mass ratio is 1, two spherical bodies with the same masses are colliding.

A separate calculation is made for each cell in Tab. 1. As described in the paragraph 2.3, for each parameter set the simulation automatically generates a cloud of points on the ellipsoid surface. Each calculation then simulates the collision of the hitting sphere at each of these points and stores the value of the maximal collision force during a particular collision. (refer Fig. 4) Thus, the number of the maximal collision force values is equal to the number of points generated on

the ellipsoid surface. Next, these values are sorted and a ratio of the smallest collision force value to the biggest collision force value is calculated and entered into each cell of Tab. 1. In this paper, this value is called collision force ratio. If the value of this collision force ratio is close to 1, this indicates that the relation of the particular geometrical dimensions or masses are not strongly influencing the collision force variation, therefore such a combination can be well approximated with bodies colliding centrally. An error made by such approximation increases with a decreasing value of the collision force ratio.

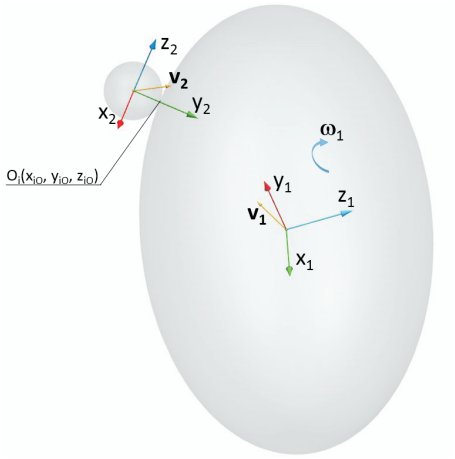

Figure 9 A sphere body hitting an ellipsoid

Table 1 Results of numerical experiment, values of collision force ratio

	0.0001	0.001	0.01	0.1	1	10	100	1000	10000
0.0001	0.350	0.350	0.351	0.381	1	0.378	0.345	0.344	0.288
0.001	0.351	0.350	0.351	0.381	1	0.378	0.345	0.344	0.288
0.01	0.352	0.352	0.352	0.382	1	0.379	0.346	0.346	0.288
0.1	0.367	0.367	0.367	0.398	1	0.379	0.361	0.361	0.288
1	0.482	0.482	0.483	0.517	1	0.513	0.476	0.456	0.288
10	0.806	0.806	0.807	0.829	1	0.821	0.699	0.456	0.288
100	0.973	0.973	0.973	0.976	1	0.922	0.699	0.456	0.288
1000	0.997	0.997	0.997	0.996	1	0.922	0.699	0.456	0.288
10000	0.999	0.999	0.999	0.997	1	0.922	0.699	0.456	0.288

3.2. *Analytical verification of numerical simulation*

To verify the results of the influence of body configuration during eccentric collision on the value of maximal impact force obtained from the numerical simulation, a theoretical case of a smooth ellipsoid of revolution hitting a body of infinite mass is analyzed. One of the semi principal axes of this ellipsoid is much bigger than the others, $a >> b, c$. The two cases shown in Fig. 10 are the subject of analysis. In both cases the ellipsoid of revolution has only a linear velocity, in first case hitting centrally and in second case at the end point. For both cases, the maximal collision force is calculated and then the ratio of the maximal force in eccentric collision to the maximal force in central collision is obtained. Several assumptions are made to simplify the calculations. It is assumed that the semi principal axes b and c are small enough in comparison with the semi principal axis a to neglect their impact in expressions for calculation of the moment of inertia. It allows, therefore, for a simplified calculation of the moment of inertia I_C as presented in the explanation of Eq. (34). Additionally, it is assumed that the force F in Case 2 is acting near the end point of the ellipsoid and is perpendicular to the ellipsoid axis. With the semi principal axis a going to an infinity, angle between axis x and ξ will go to 0, which justify such an approximation. Calculating the acceleration of the collision points in both cases is made at the start point.(Eq. (33) and Eq. (34)) During this calculation it is assumed, that the mass M is infinite.

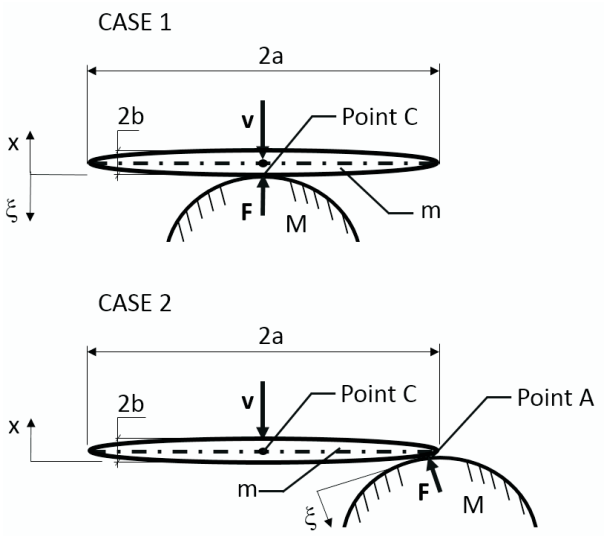

Figure 10 Ellipsoid of revolution (spheroid) hitting body with infinite mass

$$a_C = \frac{F}{m} \tag{33}$$

$$a_A = a_C + \varepsilon a = \frac{F}{m} + \frac{Fa^2}{I_c} \tag{34}$$

where:
$I_c = \frac{ma^2}{5}$ – is a inertia moment of the hitting rod
The relation given in Eq. (35) is obtained by simplifying Eq. (34)

$$a_A = \frac{F}{m_w} \tag{35}$$

where:
$m_w = \frac{m}{6}$ – is a reduced mass of colliding bodies at the collision point.
For calculation of the maximal force during the collision, the Hertz nonlinear spring model is used (Eq. (1)). The kinetic energy of the reduced system is compared with the energy stored in the local elastic deformation to obtain the maximal local deformation during the collision.

$$\frac{1}{2} m_w v_{w0}^2 = \int_0^{\xi max} k_H \xi^n d\xi \tag{36}$$

For central collision (Case 1) mass m is directly used as a reduced mass, for eccentric collision (Case 2) the expression for reduced mass is given by Eq. (35). Both values are substituted into Eq. (36) and the integral is evaluated resulting in Eq. (37) and Eq. (38), which accordingly express the maximal force in the eccentric and central collision.

$$F_{max}^{ecentric} = k_H \left[\frac{(n+1)}{2k_H} \frac{m}{6} v_{w0}^2 \right]^{\frac{n}{n+1}} \tag{37}$$

$$F_{max}^{central} = k_H \left[\frac{(n+1)}{2k_H} m v_{w0}^2 \right]^{\frac{n}{n+1}} \tag{38}$$

The ratio of the maximal force during eccentric collision to the maximal force during central collision is expressed in Eq. (39):

$$\frac{F_{max}^{ecentric}}{F_{max}^{central}} = \frac{1}{6^{\frac{n}{n+1}}} \tag{39}$$

The assumption that mass M is infinite, is an additional constraint put on the system. To verify what impact allowing mass M to have any value will have on the calculated ratio, analogical calculations to those presented above have been conducted and their result is given by Eq. (40):

$$\frac{F_{max}^{ecentric}}{F_{max}^{central}} = \left[\frac{m+M}{m+6M} \right]^{\frac{n}{n+1}} \tag{40}$$

It can also be shown, that the value of the ratio calculated from Eq. (40) tends to the value from Eq. (39) when $\frac{m}{M} \to 0$, which can happen when M is tending to infinity or m is very small Eq. (41):

$$\lim_{\frac{m}{M} \to 0} \left[\frac{m+M}{m+4M} \right]^{\frac{n}{n+1}} = \frac{1}{6^{\frac{n}{n+1}}} \tag{41}$$

For $n = 3/2$, as used in numerical simulation, Eq. (39) yields a ratio of 0.34, which is a confirmation of the results of the numerical simulation. It has larger values then those shown in the last row of Tab. 1, mostly because of the simplification made, that force F is perpendicular to semi principal axis a.

3.3. *Results of the FEM analysis*

This paragraph presents the results of the transient FEM analysis as described in paragraph 2.4. The force relation during the impact is generated by the simulation described in the paragraph 2.3. The values of the parameters for both analyses are presented in Table 2. Both the colliding bodies are made from standard carbon steel. First order tetrahedral elements are used to represent the geometry of an ellipsoid. The force pictured in Fig. 11 is applied in an opposite direction along the Y axis at the point of coordinates (0, 500, 0) (refer Fig. 9). There are no constraints put on the ellipsoid. The total time of the simulation is 0.02 s, the time step is set to 0.00001 s

Table 2 Parameters used in FEM and python simulation

Parameter description	Value of parameter
Radius of hitting sphere	50 mm
Linear velocity of hitting sphere	400 m/s
Young modulus (for ellipsoid and sphere)	$2.05*10^5$ MPa
Poisson ratio	0.3
Semi principal axes of ellipsoid	a = 2000 mm, b = 500 mm, c = 500 mm

The results of the simulation show evolution of stresses or displacements in time and can be viewed as an animation. Screens from such animation at given time are presented in Fig. 12 and Fig. 13. Both of these illustrations present reduced von Mieses stresses at given time. The stresses are given in MPa.

To validate the results of the FEM analysis, the velocity of the ellipsoid after collision is calculated analytically (refer Eq. (22)) and then compared with the FEM analysis results. The force impulse needed in Eq. (22) is obtained by calculating the area beneath the curve presented in Fig. 11. Since the ellipsoid is hit centrally, with the force vector being collinear with the Y Axis, the velocity of the ellipsoid should have only Y component. Its value calculated analytically equals: -0.0479 m/s. For the FEM analysis, the values of velocity at the point (0, 400, 250) are exported. Y component of this velocity is shown in Fig. 14.

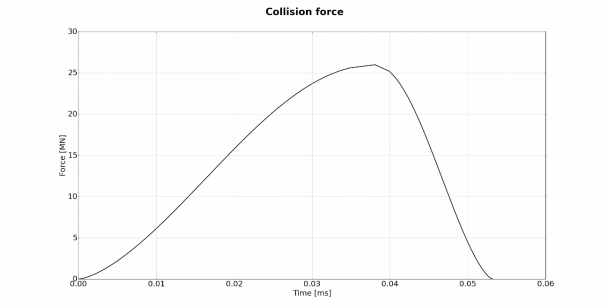

Figure 11 Collision force used in the FEM simulation

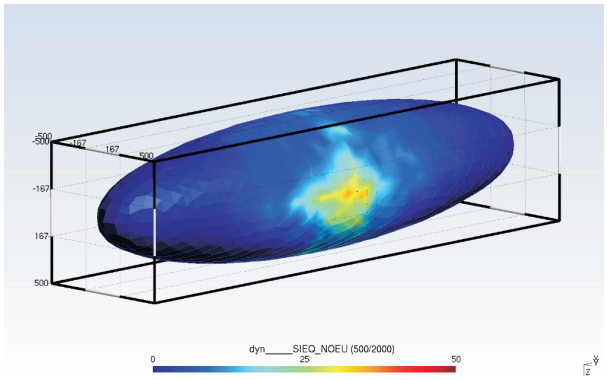

Figure 12 Results of FEM transient analysis at $t = 5$ ms

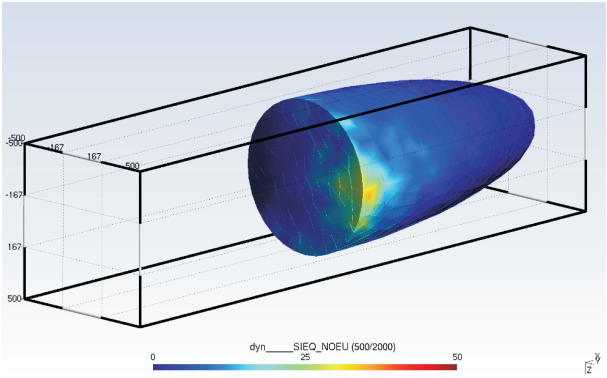

Figure 13 Cross–section at $t = 5$ ms

As the point is vibrating, its velocity is changing rapidly, but its average should correspond to the overall velocity of the ellipsoid. The average calculated from the values presented in Fig. 14 gives a value of: -0,472 m/s. The difference between both values equals 1.38 %, thus confirming the correctness of the FEM analysis.

Additionally, in Fig. 15 the values of the von Mieses reduced stresses at point (0, 400, 250) and at the point where force is applied (0, 500, 0) are presented for reference

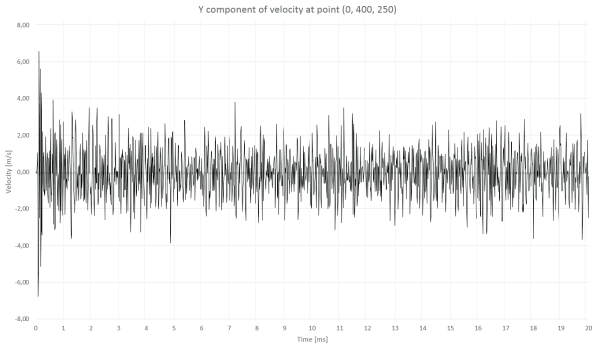

Figure 14 Y component of velocity at point (0, 400, 250)

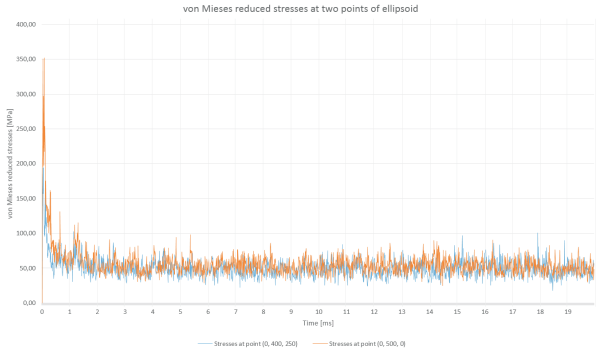

Figure 15 Von Mieses reduced stresses at two points of ellipsoid: (0, 400, 250) and (0, 500, 0)

4. Discussion

1. A closer look at Fig. 4, where the maximal forces during collision at different ellipsoid points are shown as circles with radius proportional to the maximal force value, provides a notification, that the forces at points situated on the ellipsoid principal axes of inertia do not have the same value of maximal

collision force, which at first look goes against common sense, as in such a configuration collision is central. In all these cases the reduced mass of the ellipsoid and sphere is the same and the difference is caused by the way in which the Hertz constant is calculated. (refer Eq. (1) and Eq. (**??**)). The "pointed" ends of the ellipsoid have a smaller curvature radius, which decreases the value of the calculated Hertz constant (k_H), and therefore results in lower value of the maximal collision force at these points. Thus, in the simulation, not only taking into account the kinematic parameters of the colliding bodies but also the geometric properties near to the collision point are taken into consideration.

2. Two main factors influencing the maximal collision force at a particular point in eccentric collision can be identified as: 1) the ratio of masses of colliding bodies and 2) shape of the bodies. To generalize and explain both factors in more detail two bodies, "Body 1" and "Body 2", are considered. "Body 1" has values of principal moments of inertia different from each other (for example an ellipsoid) and mass m_1. "Body 2" has values of principal moments of inertia similar to each other (for example sphere, which have equal principal moments of inertia) and mass m_2. For particular values see Table 1. If mass m2 is much bigger than mass m1, the configuration of the bodies during eccentric collision has a strong impact on the values of maximal collision. In the opposite situation, when mass m_2 is much smaller than mass m_1 the impact of the bodies configuration on maximal forces during collision is limited. First, when one of the moments of inertia of "Body 1" is much bigger than the others, the impact on the maximal collision force can be seen. The impact of the shape of the colliding bodies on the collision force at a particular point in an eccentric collision can be described by the ratio of the biggest principal moment of inertia of "Body 1" to its remaining values. With the growing value of this ratio, the impact of the configuration of the bodies is growing. Additionally, the influence of the mass ratio is declining. At the biggest ratio of principal moments of inertia, which is being investigated, the mass ratio has no impact at all.

3. An analysis of the results of the FEM simulation, as presented in Figs. 12 and 13, shows general stress levels strongly below the elasticity level (stresses observed are around 50 MPa compare with an elastic limit of 235 MPa) which supports the statement, that in the presented case the ellipsoid withstands the collision. There are stress picks observed at the initial stage of simulation, which will cause plastic deformation in the vicinity of the collision point. Contacts stresses reach high values, but proposed methodology is aimed to asses body integrity in global sense, not analyze contact phenomenon. Force applied in one point (node) and a stress averaged by an finite element much bigger in size than contact area does not allow for any analysis of contact stresses. At higher stress levels, a statement about structural integrity will require using nonlinear material behavior (material hardening curve) and eventually a damage model, which should be a subject of further investigation. For brittle materials, levels of maximal principal stresses can be used to assess material integrity.

4. An ellipsoid shape can be replaced by a technical object, for which FEM collision analysis should be conducted. The geometry created in the CAD system can be used to generate the required mesh. The CAD system can also calculate the required moments of inertia, surface curvature at collision point and vector normal to this surface at the collision point. Table 1 can be used to asses if an approximation with the central collision is justified. If not, an eccentric collision approach should be used to generate force during the collision. The calculated force relation can then be directly applied in the FEM analysis and results obtained similar to those presented in this article.

The following advantages of proposed hybrid approach deserve to be mentioned:
(I) It reduces time needed for mesh creation
(II) The FEM simulation gains direct physical justification (force function resulting from a physical model)
(III) There is no need to model contact in the FEM analysis and the problems related to it are eliminated
(IV) The calculation time is reduced as the problem has a lower number of finite elements
Also, the following disadvantages can be observed:
(I) Additional time is required to obtain the collision force function
(II) An understanding of physical phenomenon is needed for proper application of all approach steps
(III) Force applied to one point is an simplification

References

[1] **Michalczyk, J.**: Analysis of collision between axle set of a rail-vehicle & vertical unevenness of a track, *Archiwum Budowy Maszyn*, II(38), 63–73, **1991**.

[2] **Newton, I.**: Philosophia Naturalis Principia Mathematica *London: S. Pepsy, Reg. Soc.*, **1686**.

[3] **Routh, E. T.**: Dynamics of a System of Rigid Bodies, *London: MacMilan & Co.*, **1905**.

[4] **Stronge, W. J.**: Unraveling paradoxical theories for rigid body collisions, *Journal of Applied Mechanics*, IV, (58), 1049–1055, **1991**.

[5] **Bagrejev, V. V.**: Uprugo–plasticheskij udar massivnykh tel, *Trudy MIZhDT*, **1964**.

[6] **Michalczyk, J.**: Phenomenon of force impulse restitution in collision modelling, *Journal of Theoretical and Applied Mechanics*, IV, (46), 897–908, **2008**.

[7] **Gryboś, R.**: Teoria uderzenia w dyskretnych układach mechanicznych. *PWN*, **1969**.

[8] **Janin, O. and Lamarque, C. H.**: Comparsion of several numerical methods for mechanical systems with impacts, *International Journal for Numerical Methods in Engineering*, 9, (51), 1101–1132, **2001**.

[9] **Zhong, Z.H. and Mackerle, J.**: Contact-impact problems: A review with bibliography, *Applied Mechanics Reviews*, 47 (02), **1994**.

[10] **Geuzaine, C. and Remacle, J. F.**: Gmsh: a three–dimensional finite element mesh generator with built–in pre- and post–processing facilities, *International journal for numerical methods in engineering*, 79, (11), 1309–1331, **2009**.

[11] EDF. Code_Aster Documentation, (Internet: http://www.code-aster.org/V2/doc/default/en/, **2015**.

[12] **Pill, I. and Tabri, K.**: Finite element simulations of ship collisions: A coupled approach to exter nal dynamics and inner mechanics, *Analysis and Design of Marine Structures*, 103–109, **2009**.

[13] **Dubowsky, S. and Freudenstein, F.**: Dynamic analysis of mechanical systems with clearnces - Part 1: Formation of dynamical model, *Mechanics of Structures and Machines*, I, (93), 305–309, **1971**.

[14] **Brach, R. M.**: Formulation of rigid body impact problems using generalized coefficients, *International Journal of Engineering Science*, I, (36), 61-71, **1998**.

[15] **Gilardi, G. and Sharf, I.**: Literature survey of contact dynamics modeling, *Mechanism and Machine Theory*, X, (37), 1213–1239, **2002**.

[16] **Han, I.**: Multi-body impact motion with friction-analysis, simulation and experimental validation, *Journal of Mechanical Design*,III, (115), 412–422, **1993**.

[17] **Hurmuzlu, Y.**: Rigid body collision of planar kinematic chains with multiple contact points, *International Journal of Robotics Research*, I, (13), 82–92, **1994**.

[18] **Keller, J. B.**: Impact with friction, *Journal of Applied Mechanics*, I, (53), 1–4, **1986**.

[19] **Nishiura, D. and Sakaguchi, H.**: Microscopic measurements of planar viscoelastic body eccentric impacts on a convex corner, *International Journal of Non–Linear Mechanics*, 133–143, **2014**.

[20] **Stronge, W. J.**: Energy dissipated in planar collision, *Journal of Applied Mechanics*, III, (59), 681–682, **1992**.

[21] **Wang, Y. and Mason, M. T.**: Two dimensional rigid-body collisions with friction, *Journal of Applied Mechanics*, III, (59), 635–642, **1991**.

[22] **Haug, E. J., Wu, S. C. and Yang, S. M.**: Dynamics of mechanical systems with coulomb friction, stiction, impact and constraint addition-deletion, *Mechanism and Machine Theory*, V, (21), 401–406, **1986**.

[23] **Anitescu, M., Cremer, J. F. and Porta, F. A.**: Formulating three dimensional contact dynamics problems, *Mechanics of Structures and Machines*, IV, (24), 405–437, **1996**.

[24] **Lankarani, H. M. and Nikravesh, P. E.**: A contact force model with hysteresis damping for impact analysis of multi–body systems, *Journal of Mechanical Design*, 369–376, **1990**.